# DNAJC19, a Mitochondrial Cochaperone Associated with Cardiomyopathy, Forms a Complex with Prohibitins to Regulate Cardiolipin Remodeling

Ricarda Richter-Dennerlein,[1,2] Anne Korwitz,[1,2] Mathias Haag,[1,2] Takashi Tatsuta,[1,2] Sascha Dargazanli,[1,2] Michael Baker,[1,2] Thorsten Decker,[1,2] Tobias Lamkemeyer,[2] Elena I. Rugarli,[1,2,3] and Thomas Langer[1,2,3,4,*]
[1]Institute for Genetics
[2]Cologne Excellence Cluster on Cellular Stress Responses in Aging-Associated Diseases (CECAD)
[3]Center for Molecular Medicine (CMMC)
University of Cologne, 50931 Cologne, Germany
[4]Max-Planck-Institute for Biology of Aging, 50931 Cologne, Germany
*Correspondence: thomas.langer@uni-koeln.de
http://dx.doi.org/10.1016/j.cmet.2014.04.016

## SUMMARY

**Prohibitins form large protein and lipid scaffolds in the inner membrane of mitochondria that are required for mitochondrial morphogenesis, neuronal survival, and normal lifespan. Here, we have defined the interactome of PHB2 in mitochondria and identified DNAJC19, mutated in dilated cardiomyopathy with ataxia, as binding partner of PHB complexes. We observed impaired cell growth, defective cristae morphogenesis, and similar transcriptional responses in the absence of either DNAJC19 or PHB2. The loss of PHB/DNAJC19 complexes affects cardiolipin acylation and leads to the accumulation of cardiolipin species with altered acyl chains. Similar defects occur in cells lacking the transacylase tafazzin, which is mutated in Barth syndrome. Our experiments suggest that PHB/DNAJC19 membrane domains regulate cardiolipin remodeling by tafazzin and explain similar clinical symptoms in two inherited cardiomyopathies by an impaired cardiolipin metabolism in mitochondrial membranes.**

## INTRODUCTION

The function of cell organelles depends on a defined lipid composition of their membranes and a characteristic complement of embedded proteins. The diphosphoglycerolipid cardiolipin (CL) is the hallmark phospholipid of mitochondrial membranes (Osman et al., 2011). It is involved in the biogenesis of mitochondria and modulates the dynamic behavior of mitochondrial membranes and their supramolecular organization. The stability of several multiprotein complexes in both mitochondrial membranes depends on CL (Kutik et al., 2008; Pfeiffer et al., 2003; Tamura et al., 2006). Moreover, CL forms specific protein docking sites, modulating the fusion and fission of mitochondrial membranes as well as mitophagy and apoptosis (Osman et al., 2011). Mutations in the CL acyltransferase tafazzin (TAZ) cause cardiomyopathy in Barth syndrome (BTHS), revealing the pathogenic relevance of disturbances in CL metabolism (Barth et al., 1983; Bione et al., 1996; Vreken et al., 2000).

CL is synthesized along an enzymatic cascade in the inner mitochondrial membrane (IMM) from phosphatidic acid (PA), which is derived from the endoplasmic reticulum (ER). After the formation of CL at the matrix side of the IMM, structurally uniform and symmetric CL molecules are generated by TAZ-mediated remodeling of their acyl chains (Osman et al., 2011; Schlame and Haldar, 1993). Remodeling involves the formation of monolyso-CL (MLCL) and subsequent acylation by TAZ (Schlame, 2013). Loss of TAZ in BTHS leads to the accumulation of MLCL, reduced CL levels, and an altered acyl chain composition of CL and other phospholipids (Gu et al., 2004; Houtkooper et al., 2009; Schlame et al., 2003). This is accompanied by a severe functional and structural impairment of mitochondria (Acehan et al., 2007).

BTHS patients display dilated cardiomyopathy, skeletal muscle weakness, neutropenia, growth failure, hypocholesterolemia, and 3-methyl glucaconic aciduria (Barth et al., 1983; Kelley et al., 1991). Similar clinical presentations are observed in an emerging group of inherited human diseases, which includes dilated cardiomyopathy with ataxia (DCMA), MEGDEL, and Sengers syndrome. The latter two are caused by mutations in genes encoding phospholipid synthesizing enzymes in the ER or mitochondria, suggesting a pathogenic role of a disturbed membrane lipid homeostasis as in BTHS (Lamari et al., 2013; Mayr et al., 2012; Wortmann et al., 2012). DCMA, on the other hand, is associated with mutations in *Dnajc19* (Davey et al., 2006; Ojala et al., 2012). DNAJC19 is homologous to yeast Pam18/Tim14 (yPam18), a component of the mitochondrial protein import machinery in the IMM. This raises the possibility that loss of DNAJC19 in DCMA leads to defects in the import of nuclear-encoded mitochondrial proteins (Davey et al., 2006). However, experimental evidence is lacking to show such a function for DNAJC19, and therefore, the pathogenic mechanism of DCMA is still elusive.

Increasing evidence suggests that the functional integrity of mitochondrial membranes also requires a defined spatial organization of CL and other phospholipids. Proteins of the stomatin/prohibitin/flotillin/HflK/C (SPFH) family are thought to function as scaffolds in the IMM that affect the lateral distribution of

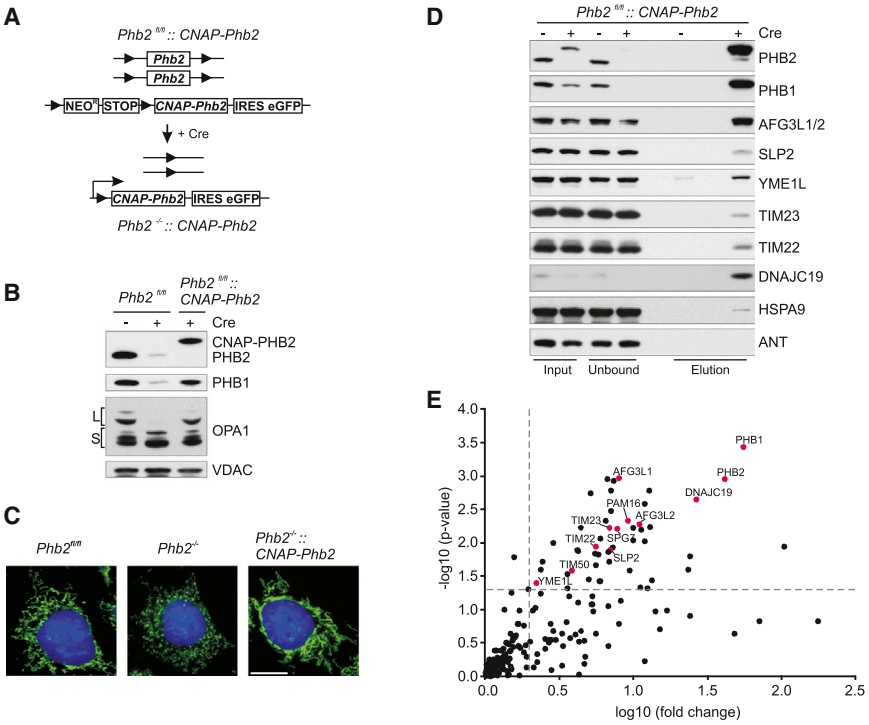


**Figure 1. Identification of PHB2 Interactors**

(A) Schematic representation of Cre-mediated *Phb2* deletion and expression of CNAP-PHB2 in *Phb2*$^{fl/fl}$*::CNAP-Phb2* cells. Cre-mediated recombination results in the deletion of the endogenous *Phb2* and the *loxP*-flanked STOP-cassette, leading to the expression of CNAP-tagged PHB2 (*Phb2*$^{-/-}$*::CNAP-Phb2*). NeoR: neomycin resistance.

(B) CNAP-PHB2 complements defects associated with loss of PHB2. Mitochondria isolated from the indicated cell lines were subjected to SDS-PAGE and immunoblotting using antibodies as indicated.

(C) CNAP-PHB2 expression maintains a tubular mitochondrial network in PHB2-deficient cells. Indicated MEFs were immunostained using antibodies against cytochrome *c* and DAPI to visualize mitochondria and the nucleus, respectively. Scale bar: 10 μm.

(D) PHB2-interacting proteins. Mitochondria isolated from *Phb2*$^{-/-}$*::CNAP-Phb2* MEFs and, for control, from untreated *Phb2*$^{fl/fl}$*::CNAP-Phb2* MEFs were subjected to metal affinity purification. Input (5%), unbound (5%), and eluate (100%) fractions were analyzed by immunoblotting using the indicated antibodies.

(E) The CNAP-PHB2 interactome identified by quantitative, label-free MS. Results from three independent experiments are presented by p values (y axis) and fold changes (x axis) on a log scale. Proteins with a fold change $\geq 2$ and a p value $\leq 0.05$ were considered for further analysis. Red dots represent proteins of the SPFH family, of the mitochondrial protein import machinery, as well as mitochondrial proteases.

both membrane lipids and proteins and thereby define functional membrane domains (Christie et al., 2011; Osman et al., 2009). Prohibitins form large, hetero-oligomeric ring complexes composed of multiple PHB1 and PHB2 subunits (Tatsuta et al., 2005). In yeast, the PHB complex interacts with the *m*-AAA protease, a quality control enzyme with important regulatory functions in the IMM (Steglich et al., 1999). Genetic interaction data link the function of PHB complexes to mitochondrial CL and phosphatidyl ethanolamine (PE) and suggest that PHB complexes cluster these phospholipids to ensure their accumulation at distinct sites in the IMM (Osman et al., 2009). Membrane domains defined by PHB complexes are essential for mitochondrial integrity and normal lifespan (Artal-Sanz and Tavernarakis, 2009). Loss of PHB complexes in mice leads to embryonic lethality and, postnatally, to the degeneration of adult neurons (Merkwirth et al., 2012) and to the loss of β cells and diabetes (Supale et al., 2013). At the cellular level, depletion of PHB complexes causes proliferation defects, destabilization of the mitochondrial genome, disturbances in mitochondrial morphology and ultrastructure, and an increased sensitivity toward apoptosis (Kasashima et al., 2008; Merkwirth et al., 2008). Many of these defects are caused by the loss of long forms of the dynamin-like GTPase OPA1 (L-OPA1) (Merkwirth et al., 2008), a central component of the mitochondrial fusion machinery.

Here, we have determined the interactome of PHB2 in the IMM to obtain comprehensive insight into the function of PHB complexes as scaffold proteins. We identified DNAJC19 as an interacting protein that functions in a complex with prohibitins. Loss of DNAJC19 or PHB complexes impairs CL metabolism and leads to an altered acyl chain composition of CL as found in TAZ-deficient cells. Our findings thus indicate that DNAJC19 functions in CL remodeling and reveal striking similarities in the molecular pathogenesis of two related cardiomyopathies, DCMA and BTHS.

## RESULTS

### Determination of the PHB2 Interactome

We established a mouse embryonic fibroblast (MEF) *Phb2*$^{fl/fl}$ cell line allowing Cre-recombinase-inducible expression of a PHB2 variant harboring an N-terminal CNAP epitope (for *c*onsecutive *n*ondenaturing *a*ffinity *p*urification) (Claypool et al., 2008). A *loxP*-flanked STOP-cassette followed by the cDNA encoding *CNAP-Phb2* was inserted into *Phb2*$^{fl/fl}$ cells (Merkwirth et al., 2008) (Figure 1A). Cre-mediated recombination resulted in simultaneous ablation of endogenous *Phb2* and ectopic expression of CNAP-PHB2, ensuring modification of all PHB2 subunits. PHB2 quantitatively assembles with PHB1 (Coates et al., 2001), which is degraded in *Phb2*$^{-/-}$ cells (Figure 1B) (Merkwirth et al., 2008). Expression of CNAP-PHB2 significantly stabilized PHB1 in *Phb2*$^{-/-}$ cells, indicating assembly of both proteins (Figure 1B). To assess the functionality of CNAP-PHB2, we monitored the morphology of mitochondria in these cells. Loss of PHB2 leads to the degradation of L-OPA1 and to fragmentation of the

**Table 1. Determination of the PHB2 Interactome by MS**

| Name | Accession | PC | PQ | p value | Max. fold change |
|---|---|---|---|---|---|
| SPFH family | | | | | |
| PHB2 | O35129 | 38 | 33 | 0.0011 | 41.64 |
| PHB1 | P67778 | 32 | 30 | 0.0004 | 55.60 |
| SLP2 | Q99JB2 | 13 | 13 | 0.0132 | 6.99 |
| Proteases | | | | | |
| AFG3L2 | Q8JZQ2 | 42 | 32 | 0.0054 | 11.13 |
| AFG3L1 | Q920A7 | 31 | 25 | 0.0011 | 8.00 |
| SPG7 | Q3ULF4 | 27 | 26 | 0.0062 | 7.87 |
| YME1L1 | O88967 | 18 | 18 | 0.0408 | 2.24 |
| Mitochondrial protein translocase | | | | | |
| DNAJC19 | Q9CQV7 | 9 | 5 | 0.0023 | 26.81 |
| PAM16 | Q9CQV1 | 7 | 7 | 0.0047 | 9.25 |
| TIMM50 | Q9D880 | 4 | 4 | 0.0263 | 3.87 |
| TIMM23 | Q9WTQ8 | 3 | 3 | 0.0061 | 6.96 |
| TIMM22 | Q9CQ85 | 2 | 2 | 0.0116 | 5.59 |
| OXPHOS | | | | | |
| NDUFS13 | Q9ERS2 | 7 | 5 | 0.0119 | 7.34 |
| NDUFS3 | Q9DCT2 | 2 | 2 | 0.0152 | 5.86 |
| NDUFA5 | Q9CPP6 | 2 | 2 | 0.0220 | 5.60 |
| NDUFA3 | Q9CQ91 | 2 | 2 | 0.0161 | 24.19 |
| NDUFC2 | Q9CQ54 | 2 | 2 | 0.0060 | 4.45 |
| UQCRC2 | Q9DB77 | 2 | 2 | 0.0048 | 6.55 |
| COX4I1 | P19783 | 4 | 4 | 0.0034 | 7.14 |
| COX6C | Q9CPQ1 | 3 | 3 | 0.0065 | 11.37 |
| COX6B1 | P56391 | 2 | 2 | 0.0059 | 12.96 |
| ATP5B | P56480 | 17 | 16 | 0.0193 | 2.45 |
| Others | | | | | |
| OCIAD1 | Q9CRD0 | 13 | 12 | 0.0097 | 11.95 |
| C2ORF47 | Q8BHE8 | 7 | 6 | 0.0381 | 6.00 |
| MTCH2 | Q791V5 | 6 | 6 | 0.0017 | 7.07 |
| SLC25A24 | Q8BMD8 | 6 | 6 | 0.0089 | 6.05 |
| C1QBQ | O35658 | 5 | 5 | 0.0130 | 4.23 |
| ATAD1 | Q9D5T0 | 5 | 5 | 0.0297 | 3.60 |
| PTRH2 | Q8R2Y8 | 3 | 3 | 0.0012 | 7.41 |
| TMEM126A | Q9D8Y1 | 3 | 3 | 0.0017 | 12.88 |
| GHITM | Q91VC9 | 3 | 3 | 0.0482 | 3.63 |
| EXOG | Q8C163 | 2 | 2 | 0.0011 | 6.71 |

Mitochondria isolated from *Phb2*$^{-/-}$*::CNAP-Phb2* MEFs were subjected to metal affinity purification. Eluate fractions of three independent experiments were analyzed by quantitative, label-free MS. PC (peptide count), number of identified peptides; PQ, peptides used for quantification $\geq 2$. Fold change $\geq 2$.

mitochondrial network (Figures 1B and 1C) (Merkwirth et al., 2008). Expression of CNAP-PHB2 in *Phb2*$^{-/-}$ cells stabilized L-OPA1 and restored a tubular, interconnected mitochondrial network, demonstrating functional complementation by CNAP-PHB2 (Figures 1B and 1C).

To define the PHB2 interactome, we isolated mitochondria from *Phb2*$^{-/-}$ cells expressing CNAP-PHB2 and purified prohibitin complexes by metal affinity chromatography (Figure 1D). Untreated *Phb2*$^{fl/fl}$*::CNAP-Phb2* cells, expressing endogenous PHB2 only, served as control. Elution fractions were analyzed by quantitative, label-free mass spectrometry (MS) (Figure 1E; Table 1). The interaction of selected binding partners with CNAP-PHB2 was verified by SDS-PAGE and immunoblotting (Figure 1D). PHB1 was highly enriched with CNAP-PHB2. Other known or expected interaction partners, including the scaffold protein SLP2 (Da Cruz et al., 2008) or all subunits of the *m*-AAA protease (AFG3L1, AFG3L2, and paraplegin/SPG7), were also copurified. Although with low efficiency, we also found the *i*-AAA protease YME1L to interact with CNAP-PHB2. The majority of other enriched proteins belong to two functional categories: subunits of OXPHOS and of the ATP synthase complexes, and subunits of the TIM22 and TIM23 translocases, which mediate the import of nuclear-encoded mitochondrial preproteins into the matrix and IMM. These findings suggest broad functions of prohibitin complexes for IMM homeostasis. The enrichment of a large number of IMM proteins with prohibitins is consistent with their proposed function as membrane scaffolds.

## DNAJC19: An Interactor of the PHB Complex

Among the most enriched proteins with CNAP-PHB2 was DNAJC19 (Figures 1D and 1E; Table 1). DNAJC19 is homologous to yPam18 and contains a conserved J-domain, which mediates the functional interaction with HSP70 chaperones by stimulating ATPase activity. However, despite high conservation within the J-domain (61% sequence identity), sequence similarities outside this domain are limited (Figure 2A). To determine the submitochondrial localization of DNAJC19, we isolated mitochondria from HEK293T cells and examined the resistance of DNAJC19 against externally added protease. DNAJC19 remained protected against proteinase K in intact mitochondria and upon osmotic disruption of the outer mitochondrial membrane (OMM) (Figure 2B). This is in contrast to TIM23 or PHB2, IMM proteins that expose domains to the intermembrane space (IMS), and to the soluble IMS protein Smac/DIABLO, but similar to mitochondrial HSP70 (HSPA9/mortalin) located in the matrix (Figure 2B). Proteinase K treatment upon disruption of mitochondrial membranes by sonication led to efficient degradation of DNAJC19 and HSPA9 (Figure 2B). In agreement with the presence of a predicted transmembrane domain (Figure 2A), DNAJC19 was recovered predominantly in the pellet fraction upon sodium carbonate extraction of mitochondrial membranes and was only released into the supernatant at high pH (Figure 2C) (Sinha et al., 2010). We therefore conclude that DNAJC19 is strongly associated with the IMM, exposing its C-terminal J-domain to the matrix space (Figure 2D).

## DNAJC19 and PAM16 Assemble into Different Complexes

yPam18 assembles with yeast Pam16/Tim16 (yPam16) and ensures protein import via TIM23 translocases into mitochondria (Frazier et al., 2004; Kozany et al., 2004; Li et al., 2004). Although less enriched than DNAJC19, various subunits of the TIM23 translocase and the mitochondrial import machinery including mammalian PAM16 were precipitated with CNAP-PHB2 (Figure 1E; Table 1), raising the possibility that DNAJC19 is required for protein import. However, we did not observe any deficiencies

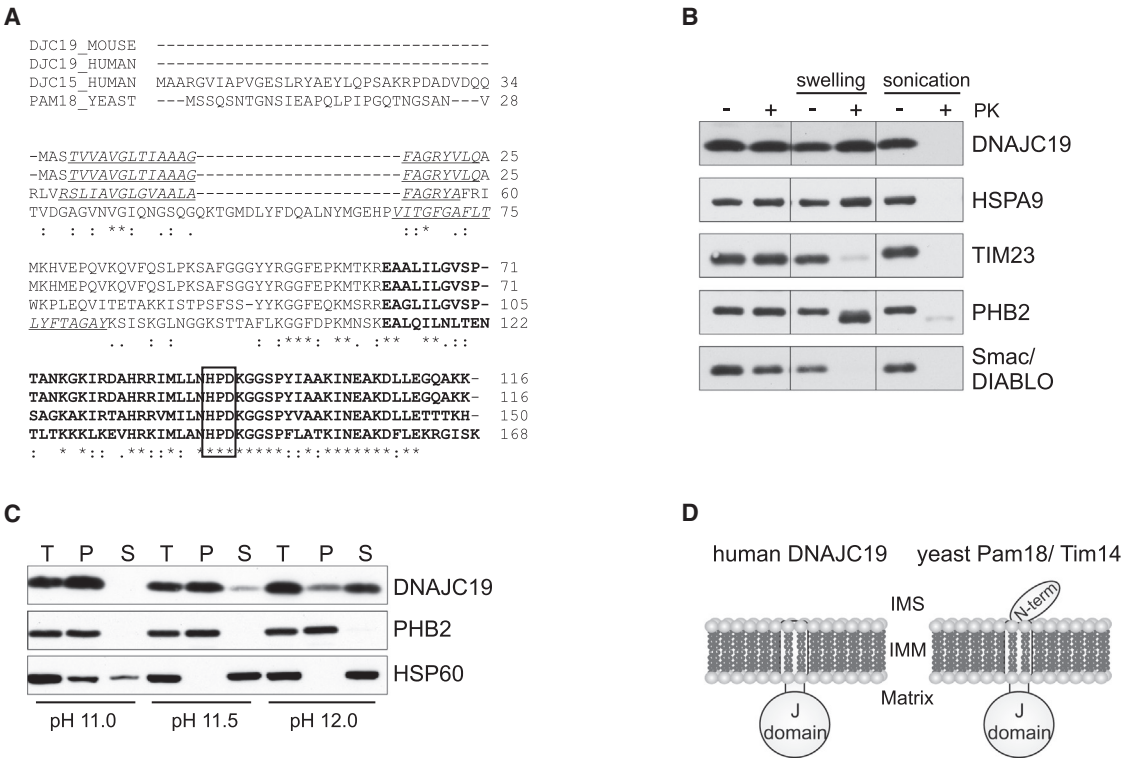


**Figure 2. Submitochondrial Localization and Membrane Topology of DNAJC19**

(A) ClustalW2 alignment of mouse and human DNAJC19 (DJC19) and of human DNAJC15 (DJC15) and yeast Pam18. Sequence identities are marked by an asterisk (*), high levels of similarity by a colon (:), and low levels of similarity by a full stop (.). The conserved J-domain containing the HPD motif (box) is depicted in bold, and the predicted transmembrane domain in italics, underlined.

(B) Human DNAJC19 localizes to the IMM. Mitochondria isolated from HEK293T cells were subjected to hypotonic swelling or sonication, treated with 50 μg/ml proteinase K where indicated, and analyzed by immunoblotting.

(C) DNAJC19 is a transmembrane protein. Mitochondria were resuspended in sodium carbonate and loaded on a sucrose cushion followed by centrifugation. Samples (T, total; P, pellet; S, supernatant) were analyzed by immunoblotting using the indicated antibodies.

(D) Schematic representation of the topology of human DNAJC19 and yeast Pam18. IMS, intermembrane space; IMM, inner mitochondrial membrane.

in protein import into mitochondria isolated from DNAJC19- or PHB2-deficient cells in vitro (Figure S1A). Consistently, DNAJC19 lacks an N-terminal domain present in yPam18 (Figures 2A and 2D), which mediates the interaction with the yeast TIM23 complex (Chacinska et al., 2005; D'Silva et al., 2008). Moreover, expression of DNAJC19 failed to restore the viability of yPam18-deficient yeast cells in recent complementation experiments (Schusdziarra et al., 2013).

It is therefore conceivable that DNAJC19 has co-opted functions in association with the PHB complex. To examine this possibility, we employed a biochemical approach in order to identify binding partners of both DNAJC19 and PAM16. We generated tetracycline-inducible HEK293T cells expressing either C-terminally FLAG-tagged DNAJC19 or C-terminally FLAG-tagged PAM16. DNAJC19$^{FLAG}$ was efficiently precipitated from mitochondrial lysates with FLAG antibodies (Figure 3A). We detected endogenous DNAJC19 in the DNAJC19$^{FLAG}$ eluates, indicating oligomerization of DNAJC19 (Figure 3A). Similarly, endogenous DNAJC19 was copurified with PAM16$^{FLAG}$, suggesting that DNAJC19 and PAM16 interact. However, when further examining DNAJC19$^{FLAG}$ and PAM16$^{FLAG}$ immunoprecipitates, we observed quantitative differences in their respective binding partners. The PHB complex as well as the *m*-AAA protease subunit AFG3L2 were precipitated with higher efficiency with DNAJC19$^{FLAG}$ than with PAM16$^{FLAG}$ (Figure 3A), which is in agreement with the 27-fold enrichment of DNAJC19 compared to a 9-fold enrichment of PAM16 in the CNAP-PHB2 purification (Table 1). We made similar observations when decreasing the expression level of DNAJC19$^{FLAG}$ to levels comparable to endogenous DNAJC19 levels (Figure S1B). Conversely, PAM16$^{FLAG}$ showed a higher affinity for TIM23 and TIM44, consistent with the predicted function of PAM16 during mitochondrial protein import (Figures 3A and S1B). We also observed more efficient binding of subunits of OXPHOS complexes III and V to PAM16 (Figure 3A). Notably, a fraction of these complexes was found to interact with TIM23 translocases in yeast (Wiedemann et al., 2007).

To directly assess the assembly of DNAJC19 and PAM16 into different oligomeric complexes, we analyzed lysates of mitochondria that were isolated from either DNAJC19$^{FLAG}$- or from PAM16$^{FLAG}$-expressing cells by blue native gel electrophoresis (BN-PAGE) (Figure 3B). Both PHB2 and AFG3L2 form large complexes of 0.8–1 MDa. Additionally, a fraction of both proteins was recovered in an even larger assembly, which represents

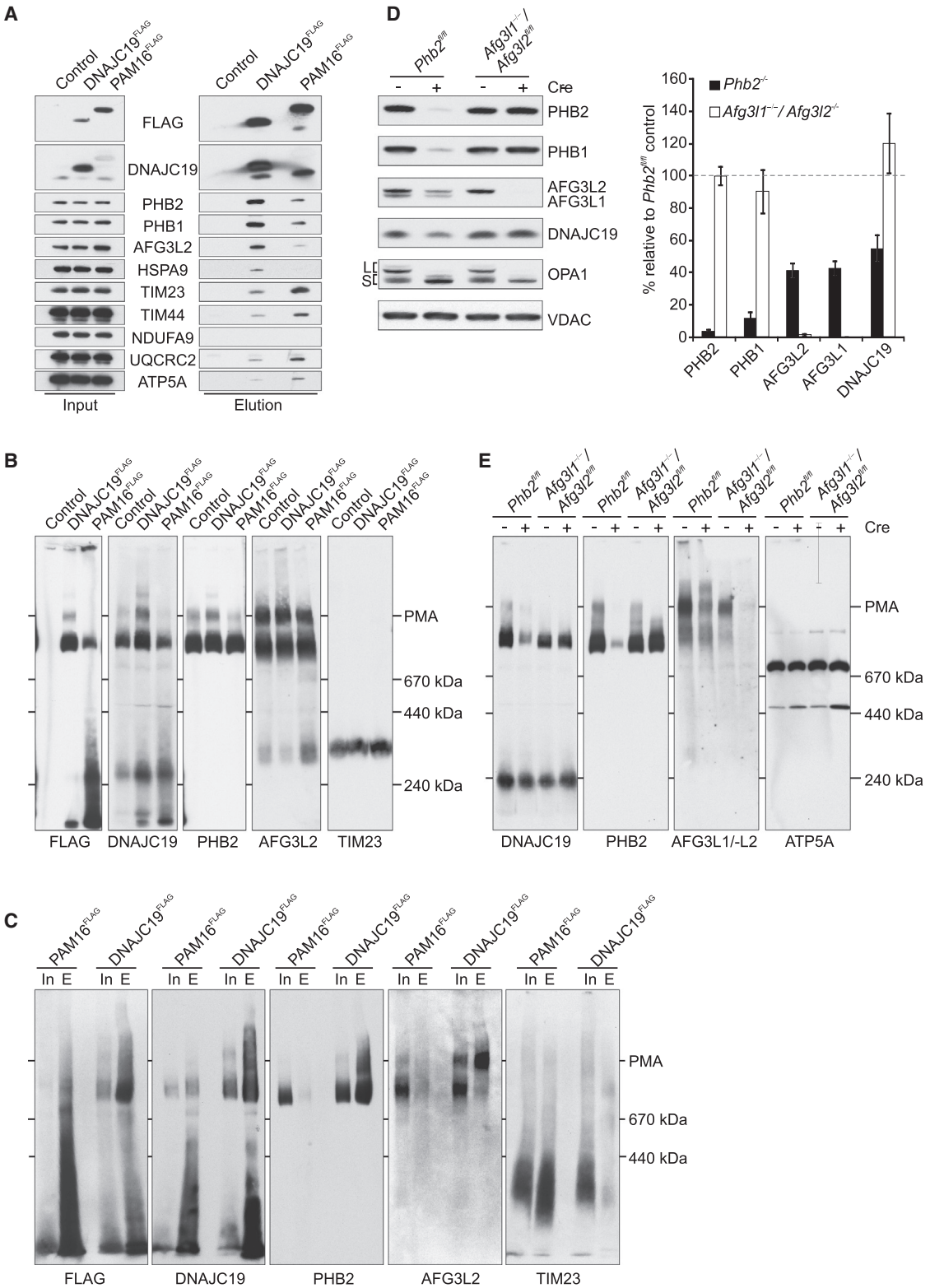


**Figure 3. DNAJC19 Forms a High-Molecular-Weight Complex with Prohibitins**

(A) Immunoprecipitation of FLAG-tagged DNAJC19 and PAM16. Mitochondria were isolated from HEK293T cells expressing DNAJC19$^{FLAG}$ or PAM16$^{FLAG}$ for 2 days (1 μg/ ml tetracycline) and solubilized with digitonin, followed by immunoprecipitation. Input (10%) and eluate (100%) fractions were analyzed by immunoblotting. Untransfected HEK293T cells were used as control.

*(legend continued on next page)*

supercomplexes of prohibitins and the *m*-AAA protease that we termed PMA (*p*rohibitin/*m*-*A*AA protease) complexes. DNAJC19$^{FLAG}$ comigrated with both PHB2-containing complexes. In agreement with these findings, endogenous DNAJC19 was predominantly found in association with PHB complexes in control cells (Figure 3B).

To substantiate these findings, we performed native immunoprecipitation experiments using cells expressing either DNAJC19$^{FLAG}$ or PAM16$^{FLAG}$. The native complexes were eluted with FLAG peptides and analyzed by BN-PAGE (Figure 3C). Immunoprecipitation of DNAJC19$^{FLAG}$ allowed efficient purification of both PHB and PMA complexes, whereas only trace amounts of TIM23 complexes were detected in the precipitate (Figure 3C). In striking contrast, TIM23 complexes but only minor amounts of PHB2 or AFG3L2 complexes were purified with PAM16$^{FLAG}$ (Figure 3C).

Taken together, these experiments identify DNAJC19 and PAM16 as part of different high-molecular-weight complexes. PAM16 mainly interacts with the TIM23 translocase, suggesting a predominant function during mitochondrial protein import. In contrast, the vast majority of DNAJC19 assembles with PHB2-containing complexes.

## Assembly of DNAJC19 with PHB Complexes Does Not Depend on the *m*-AAA Protease

The assembly of DNAJC19 with PMA complexes raises the question of whether DNAJC19 binds directly to PHB complexes or to the *m*-AAA protease. To distinguish between these possibilities, we isolated mitochondria from MEFs lacking either PHB2 (Merkwirth et al., 2008) or the *m*-AAA protease subunits AFG3L1 and AFG3L2. Cre transduction of *Phb2*$^{fl/fl}$ MEFs allowed efficient depletion of PHB2 and led to the concomitant degradation of PHB1 (Figure 3D). Interestingly, we observed significantly reduced steady-state levels of AFG3L1, AFG3L2, and DNAJC19 in these cells, pointing to a functional interdependence of these proteins (Figure 3D). In contrast, loss of the *m*-AAA protease subunits AFG3L1 and AFG3L2 did not affect the accumulation of PHB1, PHB2, or DNAJC19 (Figure 3D).

BN-PAGE analysis revealed that depletion of PHB2 from *Phb2*$^{fl/fl}$ MEFs caused an almost complete loss of assembled PHB complexes and drastically decreased the fraction of DNAJC19 present in the high-molecular-weight form (Figure 3E). Conversely, the absence of AFG3L1 and AFG3L2 did not affect the formation of PHB complexes nor their assembly with DNAJC19 (Figure 3E). We therefore conclude that DNAJC19 assembles with PHB complexes independent of the *m*-AAA protease. Consistently, PMA complexes accumulated in DNAJC19$^{FLAG}$ precipitates when compared to free *m*-AAA protease complexes (Figure 3C).

## DNAJC19 and Prohibitins Are Functionally Linked

Mutations in *Dnajc19* that are associated with DCMA lead to loss of functional protein (Davey et al., 2006; Ojala et al., 2012). We performed siRNA-mediated knockdown experiments to define roles of DNAJC19 in mitochondria and in the pathogenesis of DCMA. Similar to cells lacking PHB2 (Merkwirth et al., 2008), we observed a significantly decreased cell growth upon depletion of DNAJC19 when compared to control cells (Figure 4A). Expression of a siRNA-resistant form of DNAJC19$^{FLAG}$ restored cell growth, confirming the specificity of the siRNA and the functionality of DNAJC19$^{FLAG}$. Interestingly, DNAJC19 variants carrying mutations in the conserved HPD motif within the J-domain were not able to maintain cell growth upon depletion of endogenous DNAJC19 (Figure 4A). However, the DNAJC19$^{H90Q}$ mutant (QPD) was still able to interact with prohibitins (Figures 4B and S2). Thus, cell growth and the function of DNAJC19 depends on the J-domain of DNAJC19, which is dispensable for prohibitin binding.

Similar to the loss of PHB2, DNAJC19 depletion led to the loss of L-OPA1, which is required for mitochondrial fusion and cristae morphogenesis (Figure 4A) (Anand et al., 2014). Expression of siRNA-resistant DNAJC19$^{FLAG}$ stabilized L-OPA1, whereas L-OPA1 did not accumulate in cells expressing functionally inactive DNAJC19$^{FLAG}$ variants (Figure 4A). The metallopeptidase OMA1 mediates degradation of L-OPA1 in depolarized mitochondria (Baker et al., 2014; Ehses et al., 2009; Head et al., 2009). We therefore downregulated OMA1 by siRNA in DNAJC19-depleted cells and monitored the accumulation of L-OPA1 (Figure 4C). Depletion of OMA1 stabilized L-OPA1 in the absence of DNAJC19 (Figure 4C), demonstrating that the loss of DNAJC19 leads to activation of OMA1. However, depletion of DNAJC19 did not significantly affect the mitochondrial membrane potential, suggesting that DNAJC19 affects OMA1 activity in a different manner (Figure 4D).

The loss of L-OPA1 in PHB2-deficient cells is accompanied by the loss of mitochondrial cristae (Merkwirth et al., 2008). Consistently, we observed a disturbed mitochondrial ultrastructure in DNAJC19-depleted cells (Figure 4E). Cristae were frequently lost and appeared vesiculated rather than forming lamellar structures observed in control cells (Figure 4E). Surprisingly, downregulation of OMA1 in DNAJC19-deficient cells stabilized L-OPA1 but did not restore the mitochondrial ultrastructure (Figure 4E), indicating that other cellular defects disturb cristae morphogenesis.

The striking similarities in the phenotypes associated with the loss of DNAJC19 or PHB2 were further substantiated by gene expression profiling of DNAJC19- and PHB2-deficient cells. Heat maps of the top 100 most significantly dysregulated genes exhibited similar clustering in PHB2- and DNAJC19-depleted

(B) DNAJC19 comigrates with the PHB complex. Mitochondria isolated from HEK293T cells expressing either DNAJC19$^{FLAG}$ or PAM16$^{FLAG}$ were analyzed by BN-PAGE followed by immunoblotting.
(C) DNAJC19 assembles with prohibitins while PAM16 binds to TIM23 translocases. Complexes containing DNAJC19$^{FLAG}$ or PAM16$^{FLAG}$ were precipitated and natively eluted using 3xFLAG peptide. Input (8%) and eluate (100%) fractions were analyzed by BN-PAGE and immunoblotting.
(D) Steady-state levels of proteins in mitochondria lacking PHB or *m*-AAA protease complexes. Mitochondria were isolated from *Phb2*$^{fl/fl}$ and *Afg3l1*$^{-/-}$/*Afg3l2*$^{fl/fl}$ MEFs transduced with Cre-recombinase when indicated and analyzed by SDS-PAGE and immunoblotting. Protein levels from three independent experiments were quantified and are shown relative to mitochondria isolated from untreated *Phb2*$^{fl/fl}$ cells. Error bars indicate SD values.
(E) DNAJC19 assembles with prohibitins in the absence of the *m*-AAA protease. MEF cell lines were treated with Cre-recombinase where indicated. Mitochondrial lysates were subjected to BN-PAGE and analyzed by immunoblotting.
See also Figure S1.

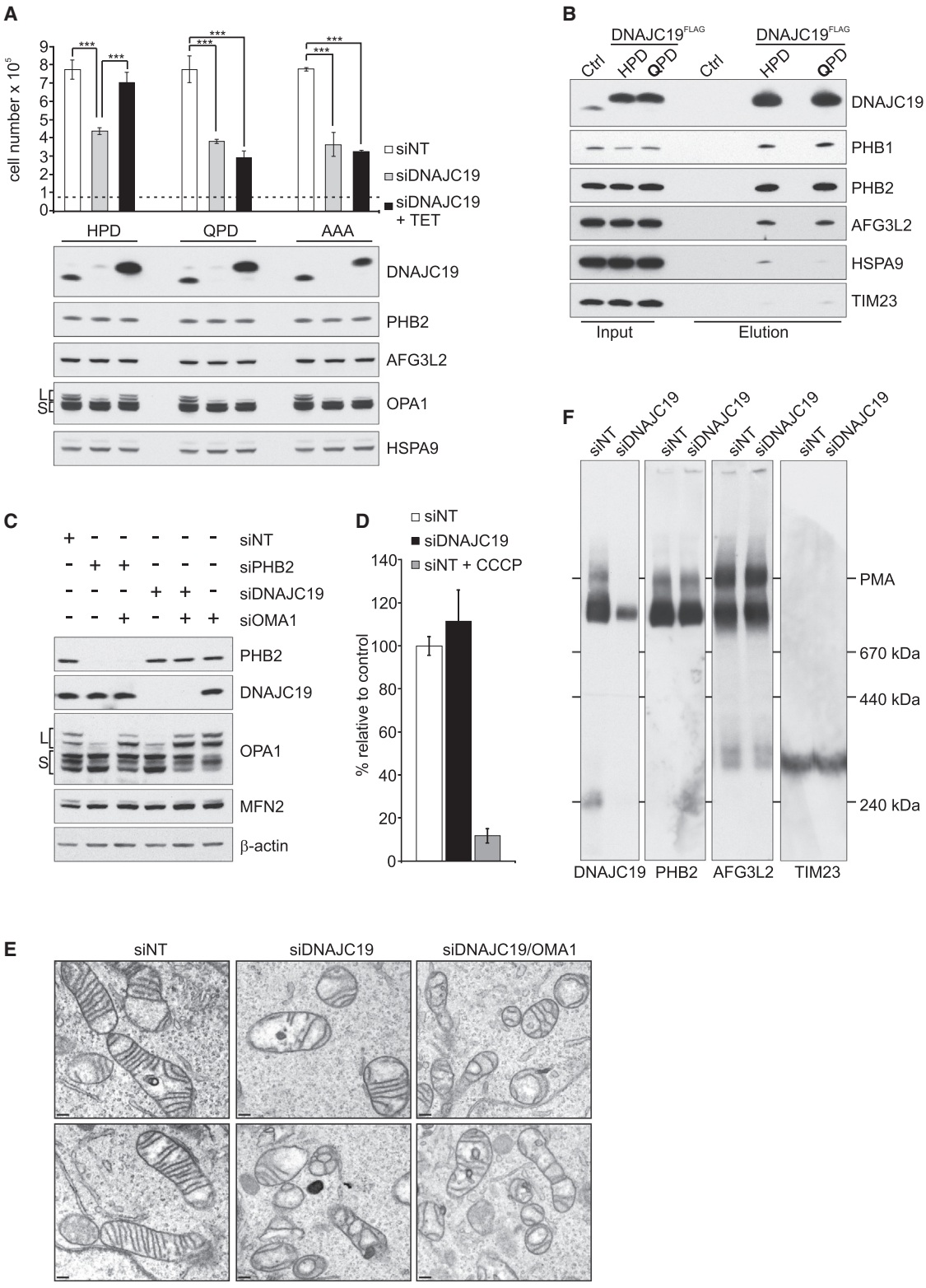


**Figure 4. DNAJC19 Depletion Affects Cell Growth, OPA1 Processing, and Mitochondrial Cristae Morphogenesis**

(A) Loss of functional DNAJC19 reduces cell growth. HEK293T cells tetracycline-inducibly expressing siRNA-resistant DNAJC19$^{FLAG}$ (HPD), DNAJC19$^{FLAG;H90Q}$ (QPD), or DNAJC19$^{FLAG;H90A;P91A;D92A}$ (AAA) were treated with control siRNA (siNT) or siDNAJC19 for 4 days. The number of cells represents the mean of three independent experiments. Starting cell number is marked as a dashed line. Relative expression levels were determined by SDS-PAGE and immunoblotting. Error bars indicate SD values. ***$p < 0.001$.

*(legend continued on next page)*

samples, suggesting a related transcriptional response (Figure S3). Pathway analyses identified the lipid metabolism, most prominently cholesterol biosynthesis, to be the most dysregulated function (Figure S3 and Table S1). Interestingly, many differentially regulated genes are under the control of SREBF1 and SREBF2 (sterol regulatory element-binding transcription factor), which are required for lipid homeostasis and are predicted to be inhibited in PHB2- and DNAJC19-depleted cells (Figure S3).

In view of the phenotypic similarities of cells lacking DNAJC19 or PHB2, it is conceivable that DNAJC19 acting as a molecular chaperone is required for the assembly of the PHB complex or its interaction with the *m*-AAA protease. To examine this possibility, we analyzed the formation of PHB complexes in DNAJC19-deficient cells by BN-PAGE. We observed assembly of both PHB and PMA complexes in mitochondria depleted of DNAJC19, indicating that DNAJC19 does not serve as an assembly factor for these complexes (Figure 4F). Thus, functional deficiencies in the absence of DNAJC19 are not caused by an impaired assembly and a functional loss of PHB complexes. Likely, DNAJC19 assembles with prohibitins in a functional complex, which is inactivated upon loss of one component.

### The Loss of DNAJC19 or TAZ Causes Similar Alterations in CL Acyl Chains

The related clinical presentations of DCMA and BTHS patients prompted us to examine the lipid composition of mitochondrial membranes lacking DNAJC19. We depleted DNAJC19 and, for comparison, TAZ in HEK293T cells, isolated mitochondria, and determined the phospholipid composition of the membranes by quantitative MS (Figure 5A). In agreement with previous findings (Gu et al., 2004; Houtkooper et al., 2009), loss of TAZ led to decreased CL levels (Figure 5A) and to accumulation of MLCL, the substrate of TAZ (Figure 5B). Depletion of DNAJC19 did not affect CL levels in mitochondrial membranes, nor did MLCL accumulate (Figures 5A and 5B). However, the acyl chain composition of CL was altered in a strikingly similar manner in the absence of DNAJC19 or of TAZ. We observed an overall tendency toward longer and less saturated acyl chains in DNAJC19- or TAZ-depleted cells (Figures 5C and 5D), as is apparent from a significant increase in the relative level of CL species with 5–7 double bonds. Notably, we observed similar alterations in the acylation of CL in cells expressing the DNAJC19$^{H90Q}$ mutant (Figures S4B–S4D). As described previously for TAZ-deficient cells (Schlame et al., 2003), acylation of other phospholipids, namely PE, phosphatidyl serine (PS), and phosphatidyl inositol (PI), was also affected in the absence of functional DNAJC19 (Figures S5C–S5F).

Taken together, these experiments demonstrate that loss of TAZ or DNAJC19 leads to strikingly similar alterations in the acyl chain composition of CL and other mitochondrial phospholipids, pointing to related pathogenic mechanisms in DCMA and BTHS. Interestingly, we observed similar alterations in CL acylation upon depletion of DNAJC19 in *Oma1*$^{-/-}$ HEK293T cells (Figures 5E and 5F), where L-OPA1 was stabilized. Moreover, loss of TAZ did not destabilize L-OPA1 (Figure S4A), although cristae morphogenesis is impaired in TAZ-deficient BTHS cells (Acehan et al., 2007). It is therefore conceivable that the altered acylation of CL and other phospholipids causes the disruption of cristae structure in these cells.

### CL Accumulation and Composition Depends on PHB Complexes

Our findings raised the possibility that PHB complexes binding DNAJC19 affect the phospholipid composition of mitochondrial membranes in a similar manner. We therefore depleted PHB2 in HEK293T cells and analyzed the phospholipid composition of mitochondrial membranes by MS. Similar to TAZ-deficient cells, CL was present at significantly reduced levels in mitochondria lacking PHB2 (Figure 6A), while MLCL slightly accumulated (Figures 6D and 6E). We observed an increase in CL species with longer and less saturated acyl chains (Figures 6B and 6C), as found in DNAJC19- or TAZ-depleted cells.

To further define at which step the PHB/DNAJC19 complex affects CL biogenesis, we examined whether the formation of MLCL in the absence of TAZ depends on DNAJC19 and PHB2 (Figure 6E). MLCL accumulated at similar levels regardless of the presence or absence of DNAJC19 or PHB2 (Figure 6E). Moreover, depletion of TAZ in cells lacking DNAJC19 or PHB2 did not lead to further alterations in the acylation of CL and other phospholipids (Figure S5). PHB/DNAJC19 complexes thus appear to affect the formation of mature CL from MLCL and may directly regulate the acylation of MLCL by TAZ.

## DISCUSSION

We have determined the interactome of mitochondrial PHB complexes and identified DNAJC19 as an interactor of these scaffold proteins. We observed alterations in the acyl chain composition of CL in the absence of DNAJC19 or PHB2 that are strikingly similar to deficiencies observed in TAZ-deficient cells. These findings therefore provide insight into the pathogenesis of DCMA and explain similarities in the clinical

(B) Binding of DNAJC19 to prohibitins does not depend on the integrity of the J-domain. Mitochondria were isolated from cells depleted of endogenous DNAJC19 and expressing DNAJC19$^{FLAG}$ (HPD) or DNAJC19$^{FLAG;H90Q}$ (QPD) followed by immunoprecipitation. Input (10%) and eluate (100%) fractions were analyzed by immunoblotting. Untransfected HEK293T cells were used as a control (Ctrl).
(C) OMA1-mediated degradation of L-OPA1 in DNAJC19-deficient cells. The accumulation of OPA1 forms was determined by SDS-PAGE and immunoblotting after 4 days of depletion of PHB2, DNAJC19, and OMA1. The levels of MFN2 remain unaffected. β-actin was used as loading control.
(D) Maintenance of mitochondrial membrane potential upon DNAJC19 depletion. HEK293T cells were treated with JC1 4 days after downregulation. Samples were analyzed by flow cytometry. Ratio of red to green fluorescence from four independent experiments was normalized to control. Error bars indicate SD values.
(E) Defective cristae morphogenesis in DNAJC19-depleted cells. Transmission electron microscopy of HEK293T cells treated with DNAJC19, OMA1, or control (siNT) siRNA. Scale bar: 0.2 μm.
(F) Assembly of PHB and PMA complexes in DNAJC19-deficient cells. Mitochondria were isolated from HEK293T cells depleted of DNAJC19 and analyzed by BN-PAGE and immunoblotting using the indicated antibodies.
See also Figure S2.

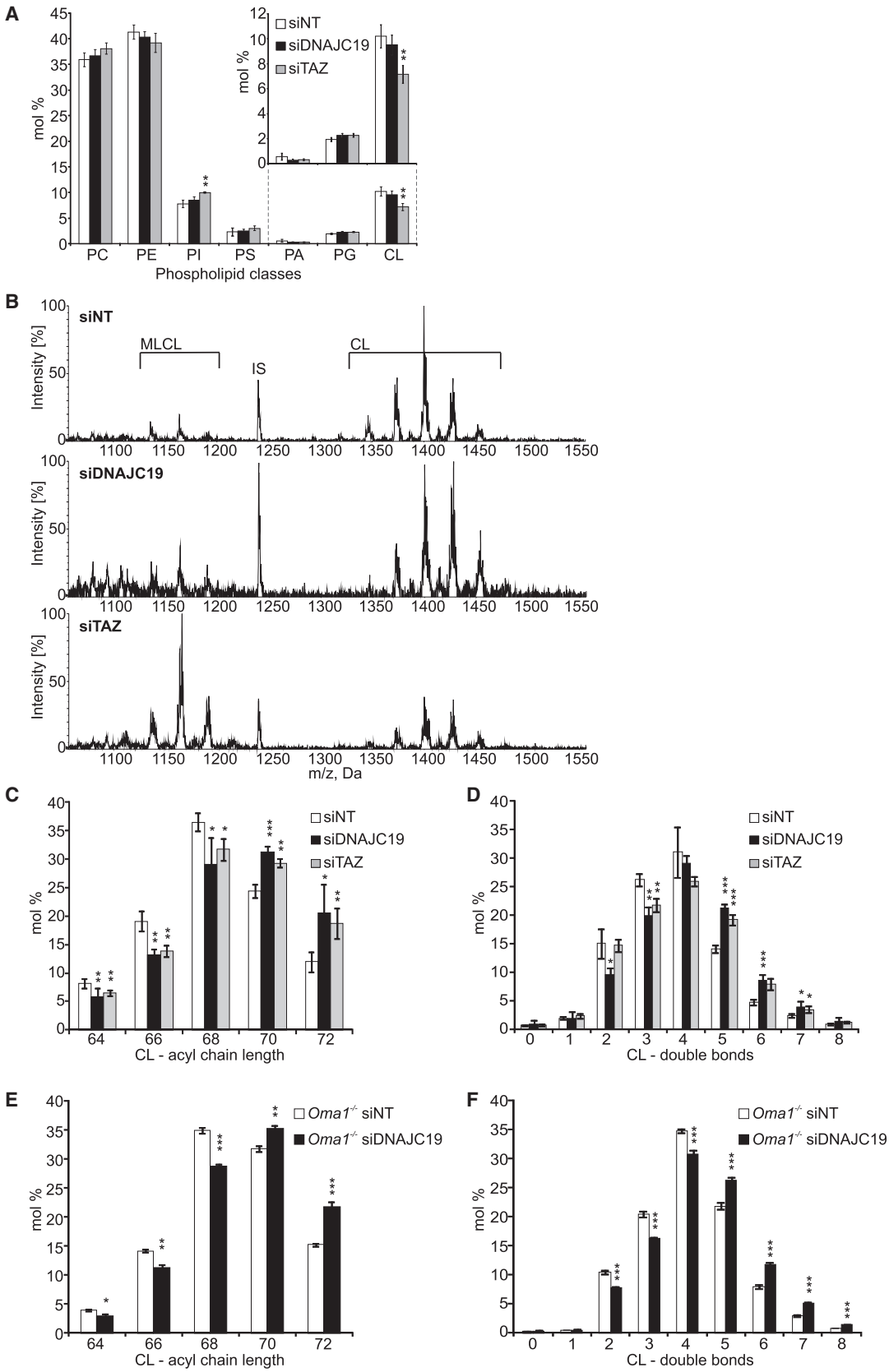


(legend on next page)

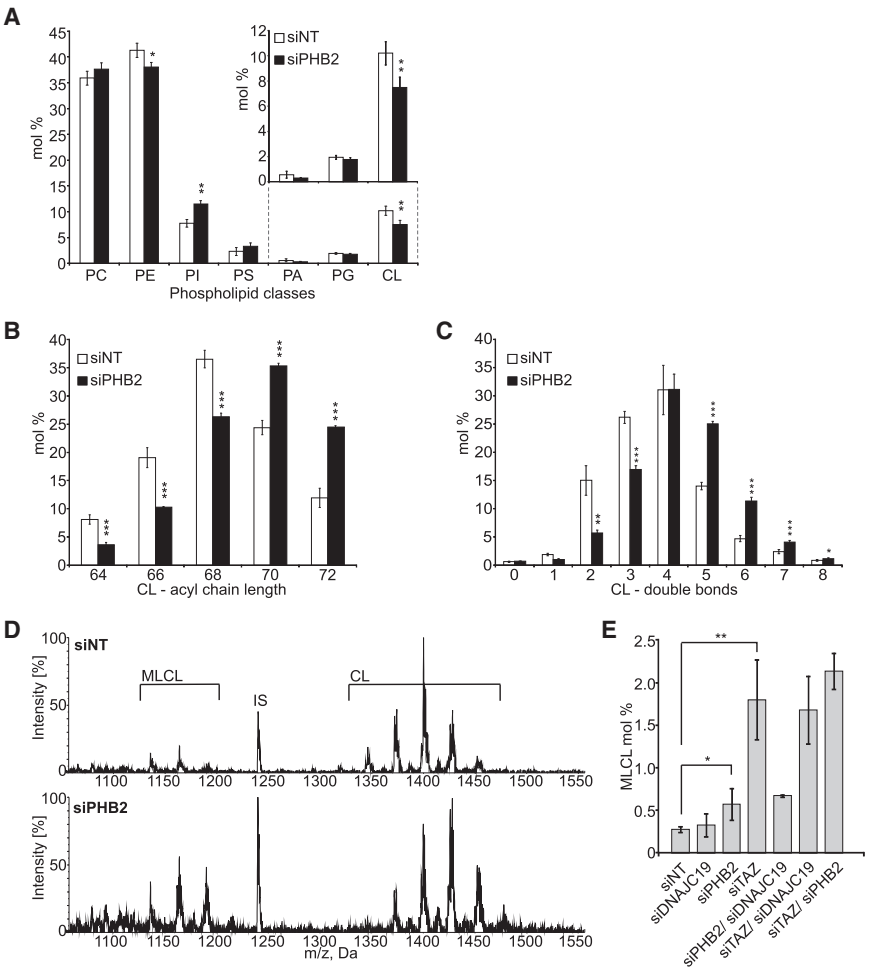


**Figure 6. PHB Complexes Ensure the Accumulation and Acylation of Mature CL**

(A) Decreased CL levels in PHB2-depleted mitochondria. The phospholipidome of mitochondria purified from PHB2-deficient cells was determined by quantitative MS. Error bars indicate SD values. n = 3; **p < 0.01.

(B and C) Accumulation of CL species with longer (B) and more unsaturated (C) acyl chains in PHB2-deficient cells. Data were analyzed as in Figures 5C and 5D. Error bars indicate SD values. n = 3; *p < 0.05; **p < 0.01; ***p < 0.001.

(D) Accumulation of MLCL in PHB2-deficient cells. Survey scans show the MS profile of MLCL and CL in PHB2-deficient and control cells. IS, internal standard.

(E) The formation of MLCL in TAZ-deficient cells does not depend on the PHB/DNAJC19 complex. Mitochondria were isolated from HEK293T cells treated with the indicated siRNAs and phospholipids were quantified by MS. Error bars indicate SD values. n = 3; *p < 0.05; **p < 0.01.

See also Figure S5.

presentations of DCMA and BTHS at the molecular level by similar alterations in the lipid composition of mitochondrial membranes.

Our biochemical analysis demonstrates that DNAJC19 associates predominantly with PHB complexes and not with TIM23 translocases, as had been suggested by the sequence similarities of DNAJC19 with yPam18 (Davey et al., 2006). This is in contrast to PAM16, which assembles with TIM23 complexes and therefore is likely involved in protein import into mitochondria. Although DNAJC19 binds to PAM16 and may contribute to the membrane translocation of mitochondrial preproteins, this appears not to be its master function. Whereas yPam18 is essential for cell survival in yeast, the loss of DNAJC19 in DCMA patients does not affect the accumulation of OXPHOS components or other mitochondrial proteins (Ojala et al., 2012). Moreover, expression of DNAJC19 fails to allow growth of Pam18-deficient yeast cells, which was restored upon expression of DNAJC15 (Schusdziarra et al., 2013), pointing to other functions of DNAJC19 in mitochondria. We observed similar functional deficiencies in the absence of DNAJC19 or PHB2, including impaired cell growth, a disturbed mitochondrial ultrastructure, and similar transcriptional responses, suggesting that the PHB/DNAJC19 complex represents the functional active structure.

How does DNAJC19 affect the functional integrity of mitochondria? Similar to PHB2, the loss of DNAJC19 triggers degradation of L-OPA1, which is required for mitochondrial fusion and the maintenance of cristae structure (Anand et al., 2014; Ishihara et al., 2006). However, stabilization of L-OPA1 upon downregulation of OMA1 did not restore normal mitochondrial cristae, suggesting that other deficiencies disturb the mitochondrial ultrastructure in the absence of DNAJC19. We observed profound alterations in the acyl chain composition of CL in these cells: longer and more unsaturated fatty acids accumulated, whereas shorter and more saturated fatty acids were decreased. These alterations are reminiscent of

**Figure 5. Altered CL Acylation in Mitochondria Lacking DNAJC19**

(A) Phospholipidome of DNAJC19-deficient mitochondria. MS analysis of mitochondrial membranes isolated from HEK293T cells treated with control siRNA (siNT), DNAJC19-, or TAZ-specific siRNA. The error bars indicate SD values. n = 3; **p < 0.01.

(B) MLCL does not accumulate upon loss of DNAJC19. Mass spectrometric profile of CL. A survey scan for precursors of m/z 152.9 was performed to determine MLCL and CL. IS, internal standard.

(C–F) Accumulation of CL species with longer (C, E) and more unsaturated (D, F) acyl chains in DNAJC19- or TAZ-deficient HEK293T cells (C, D) and *Oma1*$^{-/-}$ HEK293T cells depleted of DNAJC19. Quantity of CL species carrying acyl chains with represented number of total carbons or of double bonds were summed and then represented as a proportion in total amount of CL. Error bars indicate SD values. n = 3; *p < 0.05; **p < 0.01; ***p < 0.001.

See also Figure S4.

TAZ-deficient cells, indicating that a disturbed phospholipid homeostasis is of pathogenic relevance in DCMA as it is in BTHS. Interestingly, in contrast to cells lacking TAZ, MLCL did not accumulate in DNAJC19-deficient cells, nor was CL decreased. It thus appears that differences in acyl chains of CL and other phospholipids impair the functional integrity of mitochondrial membranes in DCMA. Consistently, we did not observe loss of L-OPA1 in TAZ-deficient cells (Figure S4A), although a disturbed mitochondrial ultrastructure was reported for BTHS lymphoblasts (Acehan et al., 2007), indicating that mitochondrial cristae alterations are caused by disturbed phospholipid homeostasis independently of L-OPA1 in both DCMA and BTHS.

Three different enzymes have been linked to CL remodeling and might therefore be affected by the loss of the PHB/DNAJC19 complex. A low MLCL acyltransferase activity has been reported for MLCLAT-1, which is identical to the C-terminal domain of the α subunit of the trifunctional protein (TFPα) (Taylor and Hatch, 2009; Taylor et al., 2012). However, we did not observe significant alterations in the accumulation of CL and MLCL nor in CL acyl chains upon depletion of TFPα (Figure S6), similar to previous findings in *Drosophila melanogaster* (Schlame et al., 2012b). Thus, DNAJC19 likely does not modulate MLCL acylation by affecting the activity of TFPα. Similarly, the activity of the acyl-CoA:lyso-CL acyltransferase (ALCAT1), which is present in mitochondria-associated ER membranes and contributes to CL acylation (Li et al., 2010), seems not to be affected by the loss of DNAJC19 or PHB2. Decreased levels of CL, altered CL acyl chains, and mitochondrial fragmentation have been observed upon overexpression of ALCAT1 (Li et al., 2010, 2012). However, in view of the localization of ALCAT1, we consider a direct effect of PHB/DNAJC19 complexes on its activity unlikely. Moreover, the altered acylation of CL in ALCAT1-deficient cells was explained by a decreased expression of MFN2 in these cells that alters phospholipid exchange between ER and mitochondria. However, we did not observe altered steady-state levels of MFN2 in DNAJC19- or PHB2-deficient cells (Figure 4C), suggesting that ALCAT1 activity remained unaffected in these cells.

We propose that DNAJC19 in complex with prohibitins regulates CL remodeling by affecting the activity of TAZ within mitochondria. The loss of DNAJC19 or PHB2 did not impair the accumulation of MLCL in the absence of TAZ, but affected the accumulation of mature CL in the presence of the acyltransferase. We did not detect a physical interaction of TAZ with DNAJC19 or PHB complexes. Rather, PHB/DNAJC19 complexes may define functional membrane domains with characteristic membrane properties, e.g., with a defined CL/MLCL ratio or membrane curvature, facilitating MLCL acylation by TAZ. In agreement with such a scenario, TAZ reacts only with a small proportion of CL in the membrane that might exhibit positive or negative curvature or be present in a nonbilayer state (Schlame et al., 2012a). CL remodeling is thought to minimize the packing energy of lipids, facilitating dynamic changes in the conformation of mitochondrial membranes (Schlame, 2013). Accordingly, alterations in the acyl chain composition of membrane lipids are likely to interfere with membrane rearrangements and may disturb the morphology of cristae in DNAJC19-deficient mitochondria. Furthermore, the defined lipid environment within a PHB membrane domain may also ensure the specificity of transacylation by TAZ, which was observed to be nonspecific in vitro (Malhotra et al., 2009) and to be confined to the specific lipid environment in vivo (Schlame et al., 2012a). The loss of PHB/DNAJC19 complexes would enable TAZ to transfer acyl chains to phospholipids other than MLCL, explaining the presence of different altered acyl chains in various mitochondrial phospholipids in the absence of PHB/DNAJC19 complexes.

Our studies reveal an unexpected function of PHB membrane scaffolds for the CL metabolism. The alterations in CL acylation, the moderately decreased CL levels, and similar transcriptional responses affecting cholesterol synthesis in PHB2-deficient cells are reminiscent of DNAJC19- and TAZ-depleted cells and make *Phb1* and *Phb2* candidate genes mutated in cardiomyopathies. Moreover, the newly identified binding partners of PHB complexes link their function to the assembly of OXPHOS complexes and protein translocases, multiprotein complexes whose assembly and stability is known to depend on CL. The PHB interactome may therefore pave the way for a deeper understanding of the mechanisms determining the supramolecular organization in the IMM and its role for mitochondrial activity, cell survival, and lifespan.

## EXPERIMENTAL PROCEDURES

### Generating Stable Cell Lines

For the generation of stable MEF cell line, SV40-transformed *Phb2*$^{fl/fl}$ MEFs (Merkwirth et al., 2008) were transfected via electroporation with pCAGs-STOP-IRES-EGFP plasmid containing murine *Phb2* cDNA with CNAP-tag at the 5′ end. One day after transfection, cells were selected with 300 μg/ml G418 for 10 days. Single G418-resistant MEF clones were isolated and expanded for further analysis. Cre protein transduction was performed as described previously (Merkwirth et al., 2008). Cells expressing CNAP-PHB2 (*Phb2*$^{-/-}$*::CNAP-Phb2*) were isolated with FACSVantage SE (Becton Dickinson) based on GFP expression upon Cre-mediated recombination in these cells.

HEK293T cells were transfected with pcDNA5-FRT-TO (with gene of interest) and pOG44 to generate stable tetracycline-inducible cell lines using GeneJuice (Novagen) as transfection reagent. Selection was started 2 days later using hygromycin (100 μg/ml). Single clones were isolated after 2 weeks' selection.

### Determination of the PHB Interactome Using CNAP-PHB2

Purification of CNAP-PHB2 was performed according to Claypool et al. (2008). Briefly, mitochondria were lysed in solubilization buffer (20 mM HEPES/KOH [pH 7.4], 20 mM imidazole/HCl [pH 7.4], 100 mM NaCl, 10% glycerol, 1 mM $CaCl_2$, Protease Inhibitor Cocktail Mix [Roche], 8 g digitonin/g protein) for 30 min prior to centrifugation for 20 min at 20,000× *g*. The supernatant was transferred to pre-equilibrated Ni-NTA Sepharose (Ni2+ Sepharose High Performance, GE). After 1.5 hr beads were washed with increasing concentrations of imidazole (20 mM, 50 mM, 100 mM, 200 mM) prior to elution with 500 mM imidazole. Samples were either analyzed by tandem mass spectrometry or TCA precipitated prior to SDS-PAGE and immunoblotting.

### Coimmunoprecipitation of FLAG-Tagged DNAJC19 and PAM16

Coimmunoprecipitation via FLAG-tag was performed using EZview Red Anti-FLAG M2 Affinity Gel (Sigma). Mitochondria were isolated from HEK293T cells expressing FLAG-tagged protein and lysed (150 mM NaCl, 50 mM Tris/HCl [pH 7.4], 2 mM EDTA, Protease Inhibitor Cocktail Mix [Roche], 4 g digitonin/g protein) prior to centrifugation for 10 min at 10,000× *g* at 4°C. Digitonin concentration of cleared supernatants was diluted to 0.4% (final concentration) prior to incubation with anti-FLAG M2 beads for 2 hr. Finally, beads were washed three times (150 mM NaCl, 50 mM Tris/HCl [pH 7.4], 2 mM EDTA,

Protease Inhibitor Cocktail Mix [Roche], 0.1% digitonin) and proteins were eluted either via pH shift with 200 mM $NH_3$ or natively with 3x FLAG peptide. Samples were further analyzed either by BN-PAGE or by SDS-PAGE followed by immunoblotting.

### Blue Native PAGE

BN-PAGE was performed as described previously with some modifications (Wittig et al., 2006). Briefly, mitochondria (100 μg) were lysed in solubilization buffer (50 mM NaCl, 5 mM 6-aminohexanoic acid, 50 mM imidazole/HCl [pH 7], 10% glycerol, 50 mM KPi-buffer [pH 7.4]) containing 8 g digitonin/g protein. Lysates or eluates from coimmunoprecipitation experiments were centrifuged, supplemented with 0.1% CBB, and separated by 3%–13% BN-PAGE.

### Mitochondria Isolation and Purification

Cells were washed in PBS and resuspended in homogenization buffer (220 mM mannitol, 70 mM sucrose, 20 mM HEPES/KOH [pH 7.4], 1 mM EDTA) containing 0.2% BSA and 1 mM PMSF. Cell suspension was homogenized with a rotating Teflon potter (Potter S, Braun) at 900 rpm followed by differential centrifugation.

For lipidome analysis, mitochondria were purified over a 40%-26%-12% percoll gradient (45 min at 56,700× *g*). Protein layers were isolated, washed with homogenization buffer, and analyzed on mitochondrial purity and integrity by immunoblotting.

### Mass Spectrometric Lipid Analysis

Mass spectrometric analysis of mitochondrial phospholipids was performed essentially as previously described (Connerth et al., 2012), with some optimization for MLCL. Lipids were extracted from percoll gradient-purified mitochondria (100 μg) in the presence of internal standards that were obtained from Avanti Polar Lipids: PC 17:0-14:1, PE 17:0-14:1, PI 17:0-14:1, PS 17:0-14:1, PG 17:0-14:1, PA 17:0-14:1, CDP-DAG 17:0-18:1, CL 14:0-14:0-14:0-14:0, and MLCL (from heart). Extraction was performed according to Bligh and Dyer with modifications. Briefly, 100 μl of 1 mg/ml mitochondria and standards are mixed with 2 ml of chloroform/methanol/25% HCl (40:80:0.6 [v/v]). After vortexing for 30 s, $H_2O$ (0.4 ml) was added followed by vortexing. After the addition of 0.5 ml chloroform and 0.5 ml $H_2O$, the sample was mixed again and phase separation was induced by centrifugation (800× *g*, 2 min). The lower chloroform phase was transferred to a second vial, and the remaining phases were washed after the addition of 0.5 ml chloroform and 0.8 ml $H_2O$. The washed chloroform phase of the second vial was transferred to a third vial, and the chloroform phase of the initial vial was combined with the aqueous phase of the second vial followed by re-extraction. After phase separation, the chloroform phases were combined and evaporated by a gentle stream of argon at 37°C. If necessary, wash step by water was omitted to increase the recovery of MLCL, and HCl was removed from the extraction solution to suppress the acid-induced deacylation of CL to MLCL during the analysis. Lipids were dissolved in 5 mM ammonium acetate and 0.05% piperidine in methanol and analyzed on a 4000 QTrap triple quadrupole mass spectrometer (Applied Biosystems, Darmstadt, Germany) equipped with a Turbo V electrospray ion source as previously described. PC, PE, PI, PS, PG, and PA species were analyzed as described (Connerth et al., 2012). CL and MLCL species were identified in negative ion mode by scanning for precursors of m/z 152.9 and quantified by MRM as singly charged ions [M-H]− at a CE of −60 eV with 100 ms dwell time. Scanned m/z and corresponding CL/MLCL species are as follows: 1239.9, CL 56:0 (internal standard); 1343.8, CL 64:4; 1345.9, CL 64.3; 1347.9, CL 64:3; 1347.9, CL 64:2; 1349.9, CL 64:1; 1369.9, CL 66:5; 1371.9, CL 66:4, 1373.9, CL 66:3, 1376.0, CL 66:2; 1398.0, CL 68:5; 1400.0, CL 68:4; 1402.0, CL 68:3; 1404.0, CL 68:2; 1422.0, CL 70:7; 1424.0, CL 70:6; 1426.0, CL 70:5; 1428.2, CL 70:4; 1430.0, CL 70:3; 1448.0, CL 72:8; 1450.0, CL 72:7; 1452.0, CL 72:6; 1454.0, CL 72:5; 1456.0, CL 72:4; 1458.0, CL 72:3; 1460.0, CL 72:2; 1462.0, CL 72:1; 1464.0, CL 72:0; 1109.9, MLCL 48:2; 1111.8, MLCL 48:1; 1134.0, MLCL 50:4; 1135.9, MLCL 50:3; 1137.9, MLCL 50:2; 1139.9, MLCL 50:1; 1161.9, MLCL 52:4; 1163.9, MLCL 52:3; 1166.0, MLCL 52:2; 1167.9, MLCL 52:1; 1186.0, MLCL 54:6; 1187.9, MLCL 54:5; 1190.0, MLCL 54:4; 1192.0, MLCL 54:3; 1193.9, MLCL 54:2. Mass spectra were processed by the LipidView Software Version 2.0 (AB Sciex, Darmstadt, Germany) for identification and quantification of lipids. Lipid amounts (pmol) were corrected for response differences between internal standards and endogenous lipids. For the analysis of length and saturation profile of the acyl chains in a phospholipid, amounts of phospholipid species carrying acyl chains with the same number of total carbons or of double bonds were summed and then represented as a proportion in total amount of the phospholipid.

### Statistical Evaluation

Means are presented with standard deviations (SD). Student's t test was performed to examine the significance of observed differences.

### Miscellaneous

Further experimental procedures can be found in the Supplemental Information.

## SUPPLEMENTAL INFORMATION

Supplemental Information includes six figures, one table, and Supplemental Experimental Procedures and can be found with this article online at http://dx.doi.org/10.1016/j.cmet.2014.04.016.

## ACKNOWLEDGMENTS

We thank Esther Barth for excellent technical support in electron microscopy and Peter Frommolt for help with the bioinformatics analysis. This work was supported by an EMBO long-term fellowship to R. R.-D. and grants of the Deutsche Forschungsgemeinschaft and the European Research Council (AdG No. 233078) to T.L.

Received: November 14, 2013
Revised: February 14, 2014
Accepted: April 10, 2014
Published: May 22, 2014

## REFERENCES

Acehan, D., Xu, Y., Stokes, D.L., and Schlame, M. (2007). Comparison of lymphoblast mitochondria from normal subjects and patients with Barth syndrome using electron microscopic tomography. Lab. Invest. *87*, 40–48.

Anand, R., Wai, T., Baker, M.J., Kladt, N., Schauss, A.C., Rugarli, E.I., and Langer, T. (2014). The i-AAA protease YME1L and OMA1 cleave OPA1 to balance mitochondrial fusion and fission. J. Cell Biol. *204*, 919–929.

Artal-Sanz, M., and Tavernarakis, N. (2009). Prohibitin couples diapause signalling to mitochondrial metabolism during ageing in C. elegans. Nature *461*, 793–797.

Baker, M.J., Lampe, P.A., Stojanovski, D., Korwitz, A., Anand, R., Tatsuta, T., and Langer, T. (2014). Stress-induced OMA1 activation and autocatalytic turnover regulate OPA1-dependent mitochondrial dynamics. EMBO J. *33*, 578–593.

Barth, P.G., Scholte, H.R., Berden, J.A., Van der Klei-Van Moorsel, J.M., Luyt-Houwen, I.E., Van 't Veer-Korthof, E.T., Van der Harten, J.J., and Sobotka-Plojhar, M.A. (1983). An X-linked mitochondrial disease affecting cardiac muscle, skeletal muscle and neutrophil leucocytes. J. Neurol. Sci. *62*, 327–355.

Bione, S., D'Adamo, P., Maestrini, E., Gedeon, A.K., Bolhuis, P.A., and Toniolo, D. (1996). A novel X-linked gene, G4.5. is responsible for Barth syndrome. Nat. Genet. *12*, 385–389.

Chacinska, A., Lind, M., Frazier, A.E., Dudek, J., Meisinger, C., Geissler, A., Sickmann, A., Meyer, H.E., Truscott, K.N., Guiard, B., et al. (2005). Mitochondrial presequence translocase: switching between TOM tethering and motor recruitment involves Tim21 and Tim17. Cell *120*, 817–829.

Christie, D.A., Lemke, C.D., Elias, I.M., Chau, L.A., Kirchhof, M.G., Li, B., Ball, E.H., Dunn, S.D., Hatch, G.M., and Madrenas, J. (2011). Stomatin-like protein 2 binds cardiolipin and regulates mitochondrial biogenesis and function. Mol. Cell. Biol. *31*, 3845–3856.

Claypool, S.M., Oktay, Y., Boontheung, P., Loo, J.A., and Koehler, C.M. (2008). Cardiolipin defines the interactome of the major ADP/ATP carrier protein of the mitochondrial inner membrane. J. Cell Biol. *182*, 937–950.

Coates, P.J., Nenutil, R., McGregor, A., Picksley, S.M., Crouch, D.H., Hall, P.A., and Wright, E.G. (2001). Mammalian prohibitin proteins respond to mitochondrial stress and decrease during cellular senescence. Exp. Cell Res. *265*, 262–273.

Connerth, M., Tatsuta, T., Haag, M., Klecker, T., Westermann, B., and Langer, T. (2012). Intramitochondrial transport of phosphatidic acid in yeast by a lipid transfer protein. Science *338*, 815–818.

D'Silva, P.R., Schilke, B., Hayashi, M., and Craig, E.A. (2008). Interaction of the J-protein heterodimer Pam18/Pam16 of the mitochondrial import motor with the translocon of the inner membrane. Mol. Biol. Cell *19*, 424–432.

Da Cruz, S., Parone, P.A., Gonzalo, P., Bienvenut, W.V., Tondera, D., Jourdain, A., Quadroni, M., and Martinou, J.C. (2008). SLP-2 interacts with prohibitins in the mitochondrial inner membrane and contributes to their stability. Biochim. Biophys. Acta *1783*, 904–911.

Davey, K.M., Parboosingh, J.S., McLeod, D.R., Chan, A., Casey, R., Ferreira, P., Snyder, F.F., Bridge, P.J., and Bernier, F.P. (2006). Mutation of DNAJC19, a human homologue of yeast inner mitochondrial membrane co-chaperones, causes DCMA syndrome, a novel autosomal recessive Barth syndrome-like condition. J. Med. Genet. *43*, 385–393.

Ehses, S., Raschke, I., Mancuso, G., Bernacchia, A., Geimer, S., Tondera, D., Martinou, J.C., Westermann, B., Rugarli, E.I., and Langer, T. (2009). Regulation of OPA1 processing and mitochondrial fusion by m-AAA protease isoenzymes and OMA1. J. Cell Biol. *187*, 1023–1036.

Frazier, A.E., Dudek, J., Guiard, B., Voos, W., Li, Y., Lind, M., Meisinger, C., Geissler, A., Sickmann, A., Meyer, H.E., et al. (2004). Pam16 has an essential role in the mitochondrial protein import motor. Nat. Struct. Mol. Biol. *11*, 226–233.

Gu, Z., Valianpour, F., Chen, S., Vaz, F.M., Hakkaart, G.A., Wanders, R.J., and Greenberg, M.L. (2004). Aberrant cardiolipin metabolism in the yeast taz1 mutant: a model for Barth syndrome. Mol. Microbiol. *51*, 149–158.

Head, B., Griparic, L., Amiri, M., Gandre-Babbe, S., and van der Bliek, A.M. (2009). Inducible proteolytic inactivation of OPA1 mediated by the OMA1 protease in mammalian cells. J. Cell Biol. *187*, 959–966.

Houtkooper, R.H., Turkenburg, M., Poll-The, B.T., Karall, D., Pérez-Cerdá, C., Morrone, A., Malvagia, S., Wanders, R.J., Kulik, W., and Vaz, F.M. (2009). The enigmatic role of tafazzin in cardiolipin metabolism. Biochim. Biophys. Acta *1788*, 2003–2014.

Ishihara, N., Fujita, Y., Oka, T., and Mihara, K. (2006). Regulation of mitochondrial morphology through proteolytic cleavage of OPA1. EMBO J. *25*, 2966–2977.

Kasashima, K., Sumitani, M., Satoh, M., and Endo, H. (2008). Human prohibitin 1 maintains the organization and stability of the mitochondrial nucleoids. Exp. Cell Res. *314*, 988–996.

Kelley, R.I., Cheatham, J.P., Clark, B.J., Nigro, M.A., Powell, B.R., Sherwood, G.W., Sladky, J.T., and Swisher, W.P. (1991). X-linked dilated cardiomyopathy with neutropenia, growth retardation, and 3-methylglutaconic aciduria. J. Pediatr. *119*, 738–747.

Kozany, C., Mokranjac, D., Sichting, M., Neupert, W., and Hell, K. (2004). The J domain-related cochaperone Tim16 is a constituent of the mitochondrial TIM23 preprotein translocase. Nat. Struct. Mol. Biol. *11*, 234–241.

Kutik, S., Rissler, M., Guan, X.L., Guiard, B., Shui, G., Gebert, N., Heacock, P.N., Rehling, P., Dowhan, W., Wenk, M.R., et al. (2008). The translocator maintenance protein Tam41 is required for mitochondrial cardiolipin biosynthesis. J. Cell Biol. *183*, 1213–1221.

Lamari, F., Mochel, F., Sedel, F., and Saudubray, J.M. (2013). Disorders of phospholipids, sphingolipids and fatty acids biosynthesis: toward a new category of inherited metabolic diseases. J. Inherit. Metab. Dis. *36*, 411–425.

Li, Y., Dudek, J., Guiard, B., Pfanner, N., Rehling, P., and Voos, W. (2004). The presequence translocase-associated protein import motor of mitochondria. Pam16 functions in an antagonistic manner to Pam18. J. Biol. Chem. *279*, 38047–38054.

Li, J., Romestaing, C., Han, X., Li, Y., Hao, X., Wu, Y., Sun, C., Liu, X., Jefferson, L.S., Xiong, J., et al. (2010). Cardiolipin remodeling by ALCAT1 links oxidative stress and mitochondrial dysfunction to obesity. Cell Metab. *12*, 154–165.

Li, J., Liu, X., Wang, H., Zhang, W., Chan, D.C., and Shi, Y. (2012). Lysocardiolipin acyltransferase 1 (ALCAT1) controls mitochondrial DNA fidelity and biogenesis through modulation of MFN2 expression. Proc. Natl. Acad. Sci. USA *109*, 6975–6980.

Malhotra, A., Xu, Y., Ren, M., and Schlame, M. (2009). Formation of molecular species of mitochondrial cardiolipin. 1. A novel transacylation mechanism to shuttle fatty acids between sn-1 and sn-2 positions of multiple phospholipid species. Biochim. Biophys. Acta *1791*, 314–320.

Mayr, J.A., Haack, T.B., Graf, E., Zimmermann, F.A., Wieland, T., Haberberger, B., Superti-Furga, A., Kirschner, J., Steinmann, B., Baumgartner, M.R., et al. (2012). Lack of the mitochondrial protein acylglycerol kinase causes Sengers syndrome. Am. J. Hum. Genet. *90*, 314–320.

Merkwirth, C., Dargazanli, S., Tatsuta, T., Geimer, S., Löwer, B., Wunderlich, F.T., von Kleist-Retzow, J.C., Waisman, A., Westermann, B., and Langer, T. (2008). Prohibitins control cell proliferation and apoptosis by regulating OPA1-dependent cristae morphogenesis in mitochondria. Genes Dev. *22*, 476–488.

Merkwirth, C., Martinelli, P., Korwitz, A., Morbin, M., Brönneke, H.S., Jordan, S.D., Rugarli, E.I., and Langer, T. (2012). Loss of prohibitin membrane scaffolds impairs mitochondrial architecture and leads to tau hyperphosphorylation and neurodegeneration. PLoS Genet. *8*, e1003021.

Ojala, T., Polinati, P., Manninen, T., Hiippala, A., Rajantie, J., Karikoski, R., Suomalainen, A., and Tyni, T. (2012). New mutation of mitochondrial DNAJC19 causing dilated and noncompaction cardiomyopathy, anemia, ataxia, and male genital anomalies. Pediatr. Res. *72*, 432–437.

Osman, C., Haag, M., Potting, C., Rodenfels, J., Dip, P.V., Wieland, F.T., Brügger, B., Westermann, B., and Langer, T. (2009). The genetic interactome of prohibitins: coordinated control of cardiolipin and phosphatidylethanolamine by conserved regulators in mitochondria. J. Cell Biol. *184*, 583–596.

Osman, C., Voelker, D.R., and Langer, T. (2011). Making heads or tails of phospholipids in mitochondria. J. Cell Biol. *192*, 7–16.

Pfeiffer, K., Gohil, V., Stuart, R.A., Hunte, C., Brandt, U., Greenberg, M.L., and Schägger, H. (2003). Cardiolipin stabilizes respiratory chain supercomplexes. J. Biol. Chem. *278*, 52873–52880.

Schlame, M. (2013). Cardiolipin remodeling and the function of tafazzin. Biochim. Biophys. Acta *1831*, 582–588.

Schlame, M., and Haldar, D. (1993). Cardiolipin is synthesized on the matrix side of the inner membrane in rat liver mitochondria. J. Biol. Chem. *268*, 74–79.

Schlame, M., Kelley, R.I., Feigenbaum, A., Towbin, J.A., Heerdt, P.M., Schieble, T., Wanders, R.J., DiMauro, S., and Blanck, T.J. (2003). Phospholipid abnormalities in children with Barth syndrome. J. Am. Coll. Cardiol. *42*, 1994–1999.

Schlame, M., Acehan, D., Berno, B., Xu, Y., Valvo, S., Ren, M., Stokes, D.L., and Epand, R.M. (2012a). The physical state of lipid substrates provides transacylation specificity for tafazzin. Nat. Chem. Biol. *8*, 862–869.

Schlame, M., Blais, S., Edelman-Novemsky, I., Xu, Y., Montecillo, F., Phoon, C.K., Ren, M., and Neubert, T.A. (2012b). Comparison of cardiolipins from Drosophila strains with mutations in putative remodeling enzymes. Chem. Phys. Lipids *165*, 512–519.

Schusdziarra, C., Blamowska, M., Azem, A., and Hell, K. (2013). Methylation-controlled J-protein MCJ acts in the import of proteins into human mitochondria. Hum. Mol. Genet. *22*, 1348–1357.

Sinha, D., Joshi, N., Chittoor, B., Samji, P., and D'Silva, P. (2010). Role of Magmas in protein transport and human mitochondria biogenesis. Hum. Mol. Genet. *19*, 1248–1262.

Steglich, G., Neupert, W., and Langer, T. (1999). Prohibitins regulate membrane protein degradation by the m-AAA protease in mitochondria. Mol. Cell. Biol. *19*, 3435–3442.

Supale, S., Thorel, F., Merkwirth, C., Gjinovci, A., Herrera, P.L., Scorrano, L., Meda, P., Langer, T., and Maechler, P. (2013). Loss of prohibitin induces mitochondrial damages altering β-cell function and survival and is responsible for gradual diabetes development. Diabetes *62*, 3488–3499.

Tamura, Y., Harada, Y., Yamano, K., Watanabe, K., Ishikawa, D., Ohshima, C., Nishikawa, S., Yamamoto, H., and Endo, T. (2006). Identification of Tam41 maintaining integrity of the TIM23 protein translocator complex in mitochondria. J. Cell Biol. *174*, 631–637.

Tatsuta, T., Model, K., and Langer, T. (2005). Formation of membrane-bound ring complexes by prohibitins in mitochondria. Mol. Biol. Cell *16*, 248–259.

Taylor, W.A., and Hatch, G.M. (2009). Identification of the human mitochondrial linoleoyl-coenzyme A monolysocardiolipin acyltransferase (MLCL AT-1). J. Biol. Chem. *284*, 30360–30371.

Taylor, W.A., Mejia, E.M., Mitchell, R.W., Choy, P.C., Sparagna, G.C., and Hatch, G.M. (2012). Human trifunctional protein alpha links cardiolipin remodeling to beta-oxidation. PLoS ONE *7*, e48628.

Vreken, P., Valianpour, F., Nijtmans, L.G., Grivell, L.A., Plecko, B., Wanders, R.J., and Barth, P.G. (2000). Defective remodeling of cardiolipin and phosphatidylglycerol in Barth syndrome. Biochem. Biophys. Res. Commun. *279*, 378–382.

Wiedemann, N., van der Laan, M., Hutu, D.P., Rehling, P., and Pfanner, N. (2007). Sorting switch of mitochondrial presequence translocase involves coupling of motor module to respiratory chain. J. Cell Biol. *179*, 1115–1122.

Wittig, I., Braun, H.P., and Schägger, H. (2006). Blue native PAGE. Nat. Protoc. *1*, 418–428.

Wortmann, S.B., Vaz, F.M., Gardeitchik, T., Vissers, L.E., Renkema, G.H., Schuurs-Hoeijmakers, J.H., Kulik, W., Lammens, M., Christin, C., Kluijtmans, L.A., et al. (2012). Mutations in the phospholipid remodeling gene SERAC1 impair mitochondrial function and intracellular cholesterol trafficking and cause dystonia and deafness. Nat. Genet. *44*, 797–802.